


Genomic Rearrangements in Arabidopsis Considered as Quantitative Traits

Journal Article

Author(s):

Imprialou, Martha; Kahles, André; Steffen, Joshua G.; Osborne, Edward J.; Gan, Xiangchao; Lempe, Janne; Bhomra, Amarjit; Belfield, Eric; Visscher, Anne; Greenhalgh, Robert; Harberd, Nicholas P.; Goram, Richard; Hein, Jotun; Robert-Seilaniantz, Alexandre; Jones, Jonathan; Stegle, Oliver; Kover, Paula; Tsiantis, Miltos; Nordborg, Magnus; [Rätsch, Gunnar](#) ; Clark, Richard M.; Mott, Richard

Publication date:

2017-04

Permanent link:

<https://doi.org/10.3929/ethz-b-000191854>

Rights / license:

[Creative Commons Attribution 4.0 International](#)

Originally published in:

Genetics 205(4), <https://doi.org/10.1534/genetics.116.192823>

Genomic Rearrangements in *Arabidopsis* Considered as Quantitative Traits

Martha Imprialou,^{*,†} André Kahles,[‡] Joshua G. Steffen,[§] Edward J. Osborne,[§] Xiangchao Gan,^{**}
Janne Lempe,^{**} Amarjit Bhomra,^{*} Eric Belfield,^{**} Anne Visscher,^{††,‡‡} Robert Greenhalgh,[§]
Nicholas P Harberd,^{††} Richard Gorum,^{§§} Jotun Hein,[†] Alexandre Robert-Seilaniantz,^{***} Jonathan Jones,^{†††}
Oliver Stegle,^{†††} Paula Kover,^{§§§} Miltos Tsiantis,^{**} Magnus Nordborg,^{****} Gunnar Rättsch,^{*}
Richard M. Clark,^{§,††††} and Richard Mott^{††††,1}

^{*}Wellcome Trust Centre for Human Genetics, [†]Department of Statistics, and ^{††}Department of Plant Sciences, University of Oxford, OX1 3RB, United Kingdom, [‡]Department of Computer Science, Swiss Federal Institute of Technology in Zurich, 8092, Switzerland, [§]Department of Biology and ^{††††}Center for Cell and Genome Science, University of Utah, Salt Lake City, Utah 84112-0840, ^{**}Department of Comparative Development and Genetics, Max Planck Institute for Plant Breeding Research, 50829 Köln, Germany, ^{†††}Department of Comparative Plant and Fungal Biology, Royal Botanic Gardens Kew, Ardingly RH17 6TN, United Kingdom, ^{§§}John Innes Centre, Norwich NR4 7UH, United Kingdom, ^{***}UMR INRA-Agrocampus Ouest-Université de Rennes 1, 35653 Le Rheu Cedex, France, ^{††††}The Sainsbury Laboratory, Norwich Research Park, NR4 7UH, United Kingdom, ^{††††}European Bioinformatics Institute, Hinxton, Cambridge CB10 1SD, United Kingdom, ^{§§§§}Department of Biology and Biochemistry, University of Bath, BA2 7AY, United Kingdom, ^{****}Department of Population Genetics, Gregor Mendel Institute of Molecular Plant Biology, 1030 Vienna, Austria, and ^{††††}UCL Genetics Institute, University College London, WC1 6BT, United Kingdom

ORCID IDs: 0000-0002-3411-0692 (A.K.); 0000-0001-6398-5191 (X.G.); 0000-0002-8100-0824 (J.H.); 0000-0002-4953-261X (J.J.); 0000-0002-8818-7193 (O.S.); 0000-0001-7178-9748 (M.N.); 0000-0001-5486-8532 (G.R.); 0000-0002-1470-301X (R.M.C.); 0000-0002-1022-9330 (R.M.)

ABSTRACT To understand the population genetics of structural variants and their effects on phenotypes, we developed an approach to mapping structural variants that segregate in a population sequenced at low coverage. We avoid calling structural variants directly. Instead, the evidence for a potential structural variant at a locus is indicated by variation in the counts of short-reads that map anomalously to that locus. These structural variant traits are treated as quantitative traits and mapped genetically, analogously to a gene expression study. Association between a structural variant trait at one locus, and genotypes at a distant locus indicate the origin and target of a transposition. Using ultra-low-coverage (0.3×) population sequence data from 488 recombinant inbred *Arabidopsis thaliana* genomes, we identified 6502 segregating structural variants. Remarkably, 25% of these were transpositions. While many structural variants cannot be delineated precisely, we validated 83% of 44 predicted transposition breakpoints by polymerase chain reaction. We show that specific structural variants may be causative for quantitative trait loci for germination and resistance to infection by the fungus *Albugo laibachii*, isolate Nc14. Further we show that the phenotypic heritability attributable to read-mapping anomalies differs from, and, in the case of time to germination and bolting, exceeds that due to standard genetic variation. Genes within structural variants are also more likely to be silenced or dysregulated. This approach complements the prevalent strategy of structural variant discovery in fewer individuals sequenced at high coverage. It is generally applicable to large populations sequenced at low-coverage, and is particularly suited to mapping transpositions.

KEYWORDS structural variation; *Arabidopsis*; quantitative trait locus; heritability; low-coverage sequencing

WHILE genome resequencing can readily determine variations such as Single Nucleotide Polymorphisms (SNPs) and small indels, it remains challenging to identify structural variants (SVs) and rearrangements, despite improvement in algorithms for calling SVs. The current gold standard for determining SVs between individuals is by *de novo* assembly (Simpson and Pop 2015). This requires

high-coverage paired-end sequence over a range of insert sizes, together with long-range information such as from long-read technologies (Chaisson and Tesler 2012; Jain *et al.* 2015) for scaffolding. The high cost and low throughput of *de novo* assembly limit its use, and leaves open two important questions. First, whether an SV is identified in an individual frequently enough to contribute to phenotypic

heritability in a population. Second, whether an SV represents a local rearrangement, such as a deletion, inversion or tandem copy-number variant (CNV), or is long-range, such as a transposition (Cao *et al.* 2011; Mills *et al.* 2011).

SVs are frequently revealed by the anomalous alignment of short-reads to the reference genome. Specific anomaly signatures characterize different types of SVs (Table 1). Thus, same-strand pairs indicate inversion, high read coverage duplications, abnormal insert sizes, and unpaired reads indels (Figure 1). These anomalies arise, often in combination, because the reads have been aligned to the wrong genome—the anomalies disappear if instead the reads are aligned to the true genome. This idea is used by algorithms such as GATK (McKenna *et al.* 2010) and Platypus (Rimmer *et al.* 2014) that identify small indels by local realignment, and in whole-genome reassembly by iterative realignment (Gan *et al.* 2011).

Many SV-calling algorithms utilize read-anomaly signatures to identify SVs segregating in individuals sequenced at high coverage (Chen *et al.* 2009; Manske and Kwiatkowski 2009; Ye *et al.* 2009; Simpson *et al.* 2010; Rausch *et al.* 2012; Sindi *et al.* 2012; Layer *et al.* 2014; Kronenberg *et al.* 2015). They focus on short-range SVs because of the difficulties in distinguishing long-range rearrangements from read mapping errors. They also work best when calling SVs in individuals sequenced at intermediate to high coverage; for example, LUMPY (Layer *et al.* 2014) and WHAM (Kronenberg *et al.* 2015) are most sensitive at coverage $>10\times$. In other applications, *e.g.*, cancer resequencing, typical coverage is even higher, at $30\times$ or above.

Further challenges arise when calling SVs in large samples of population sequence data, for the purpose of testing genetic association. Population sequencing provides an alternative to genotyping by SNP arrays, simultaneously providing both haplotype reference panels for imputation (Durbin *et al.* 2010), and cohorts for disease mapping (Cai *et al.* 2015; Nicod *et al.* 2016). As the sample size increases, the coverage of each individual may be reduced without affecting imputation accuracy (Davies *et al.* 2016). Although the information present in each sample is then sparse, and therefore it would be difficult to call SVs (and even SNPs) on an individual basis, by pooling information across samples it might be possible to determine common SVs analogously to the way SNPs are imputed.

In addition to simple indels, inversions, and transpositions, where a segment with well-defined breakpoints is affected, many SVs are composites of multiple events (Yalcin *et al.* 2011), often driven by transposons and other mobile

elements. These complex SVs resist simple classification, and the precise sequence of mutations that occurred may be unrecoverable. While current algorithms for calling SVs in simulated high-coverage human data can identify simple SVs with sensitivities of $\sim 90\%$ depending on the type of SV (Kronenberg *et al.* 2015), they are less accurate when applied to real data, and their performance on complex SVs is unreported.

Despite this, there may still be strong evidence from read-mapping anomalies that an SV of some sort segregates at a locus. Furthermore, if the intensity of its anomaly signature can be used as a proxy for the purposes of testing genetic association, then one need not call the SV precisely. It then follows that information encoded by these anomalies across the genome could be used to compute relationships between individuals based on their structural profiles alone, and hence to estimate the heritability attributable to structural variation directly.

Here, we show how low-coverage population sequencing provides new ways for mapping SVs and estimating heritability, complementing the sequencing of fewer individuals at high coverage. As an illustration, we investigate the architecture and phenotypic impact of structural variation in *Arabidopsis thaliana*. Among natural accessions of *Arabidopsis*, structural variation is plentiful (Cao *et al.* 2011). The extent of rDNA repeats (Hu *et al.* 2011) and mobile transposable elements (Quadrona *et al.* 2016) vary between accessions, and variation in the overall amounts of both classes of repetitive sequence elements are complex traits, partially under genetic control. In this study we investigate all types of structural variation in *Arabidopsis*, including those not mediated by mobile elements. We show that long-range transpositions are common, and that structural variation has a significant impact on particular quantitative trait loci (QTL) and on trait heritability, distinct from that explained by other types of sequence variation.

Materials and Methods

DNA extraction and sequencing

Multiparent Advanced Generation Inter-Cross (MAGIC) lines were grown at Bath (laboratory of P.K.) or Oxford (laboratory of N.P.H.) in greenhouses or growth chambers, respectively. Leaves were harvested for DNA extraction. DNA isolation was performed at the John Innes Centre, in 96-well plates using the DNeasy 96 Plant Kit and DNeasy 96 Protocol (<http://www.qiagen.com>). Sequencing was performed by the Oxford Genomics Centre.

Genomic DNA library construction and multiplexing

Samples were quantified using the Quant-iT PicoGreen dsDNA Kits (Invitrogen, Carlsbad, CA) and a Genios plate scanner (Tecan, Männedorf, Switzerland) according to manufacturer specifications. Sample integrity was assessed using 1% agarose gel. DNA (~ 300 ng) was fragmented using a

Table 1 MAGIC SV-QTL classified by read pair anomaly type and QTL type, after removing duplicates

	SV-QTL	Unique	<i>Cis</i>	<i>Trans</i>
Trait type				
IP	1,997	833	1617	380
ER	184	165	112	72
LIS	2,051	585	1677	374
SS	1,950	1887	1358	592
U	2,060	1998	1530	530
U+LIS	2,033	431	1661	372
Total	10,275	5899	7955	2320
SV type				
Duplication	175		109	66
Indel	3,035		3035	0
Inversion	1,976		1373	603
Other	1,316		381	935
Total	6,502		4898	1604

SV-QTL: total number of QTL detected using each anomaly type. If the same QTL is detected by multiple anomalies then it is counted multiple times in this column). Unique: number of QTL detected after counting duplicates only once. *cis*: number of *cis* SV-QTL (source and sink within 2 Mb from each other), *trans*: number of *trans* SV-QTLs. Note that the total number of SV-QTL is 10,275, of which 6502 are distinct after removing overlapping events, and 5899 unique to a single anomaly type. IP, improperly paired; ER, excess reads; LIS, large insert size; SS, same strand; U, unmapped; U_LIS, unmapped or large insert size.

Covaris S2 system with the following settings: Intensity: 5, Duty Cycle: 20, Cycles per Burst: 200, Time: 60 sec. Distribution of fragments after shearing was determined using a TapeStation D1200 system (Agilent/Lab901, Santa Clara, CA). DNA Libraries were constructed using the NEBNext DNA Sample Prep Master Mix Set 1 Kit (New England Biolabs, Beverly, MA), with minor modifications, and a custom automated protocol on a Biomek FX (Beckman, Fullerton, CA). Ligation of adapters was performed using Illumina Adapters (Multiplexing Sample Preparation Oligonucleotide Kit). Ligated libraries were size selected using Ampure magnetic beads (Agencourt, Beckman, Fullerton, CA). Each library was PCR enriched with 25 μ M each of the following custom primers:

Multiplex PCR primer 1.0

5'-AATGATACGGCGACCACCGAGATCTACACTCTTTCCCTA
CACGACGCTCTTCCGATCT-3'

Index primer

5'-CAAGCAGAAGACGGCATAACGAGAT[INDEX]CAGTGACTG
GAGTTTACAGCGTGTGCTCTTCCGATCT-3'

Indexes used were 8 bp long. Enrichment and adapter extension of each preparation was obtained using 5 μ l of size-selected library in a 50 μ l PCR reaction. After 10 cycles of amplification (cycling conditions as per Illumina recommendations), the reactions were purified with Ampure beads (Agencourt/Beckman). The final size distribution was determined using a TapeStation 1DK system (Agilent/Lab901). The concentrations used to generate the multiplex pool were determined by Picogreen. The library resulting from the pooling was quantified using the Agilent qPCR Library Quantification Kit and a MX3005P instrument (Agilent)

before sequencing on an Illumina GAIIx as 50 or 100 bp paired-end reads. All steps for library construction, including the setup of the PCR reaction were performed on a Biomek FX (Beckman). Post PCR cleanup was carried out on a Biomek NXp (Beckman) whereas a Biomek 3000 (Beckman) was used to generate the pools of 96 indexed libraries.

Processing sequence reads and SNP calling

The Illumina reads were mapped to the *A. thaliana* reference (TAIR10) using Stampy v1.0.20 (Li and Durbin 2010; Lunter and Goodson 2011). Alignments were stored in a separate BAM file for each MAGIC line. Previous sequencing for the 18 MAGIC line progenitors had produced a catalog of 3,316,270 segregating SNPs (Gan *et al.* 2011). We ran GATK v2.6 (McKenna *et al.* 2010) on the segregating SNPs to call variants for the 19 founders, setting the following read filters: Allele Balance, BaseQualityRankSumTest, Clipping RankSumTest, Coverage, DepthPerAlleleBySample, FisherStrand, GCContent, HaplotypeScore, LowMQ, MappingQualityRankSumTest, MappingQualityZero, MappingQualityZeroBySample, RMSMappingQuality, and ReadPosRankSumTest. We filtered out SNPs that were triallelic, within annotated transposons, or heterozygous for any founders.

Definition of structural variant traits

We divided the TAIR10 reference genome into 11,915 abutting 10 kb segments. Within each segment, we computed six measures of anomalously mapped reads that are signatures of SVs. Let R be the set of all reads mapped to a genome of length L ; ρ is the number of reads in R , and ρ_l the number of reads mapped to a segment l of length 10 kb. The read anomaly measures computed in each segment are:

1. High read coverage: $\rho_{hc} = \rho_l - 1.5E[\rho_l]$, where $E[\rho_l] = (\rho \times l)/L$ is the expected read coverage of the segment
2. Unpaired reads: ρ_u number of reads mapping to the segment whose pair is not mapped
3. Pairs on the same strand: ρ_s number of reads with pair on the same strand
4. Reads with large insert size: ρ_{is} number of read pairs with insert size outside the range $m_s \pm IQR_s$, or mapped to different chromosomes, m_s, IQR_s being the median and interquartile range of insert sizes of all the reads in the sample.
5. Unpaired reads or with large insert size: $\rho_{ui} = \rho_u + \rho_i$
6. Improperly paired reads: $\rho_{uis} = \rho_u + \rho_i + \rho_s$

The last two traits are combination of others—certain SV types can cause multiple anomaly signatures, so merging them may increase power. Each type of read pair anomaly was measured in each of the 11,915 10 kb segments, determining 71,490 traits in total.

Genome scans

We treated the SV traits like a gene expression eQTL study, performing a genome scan for each one. Association was

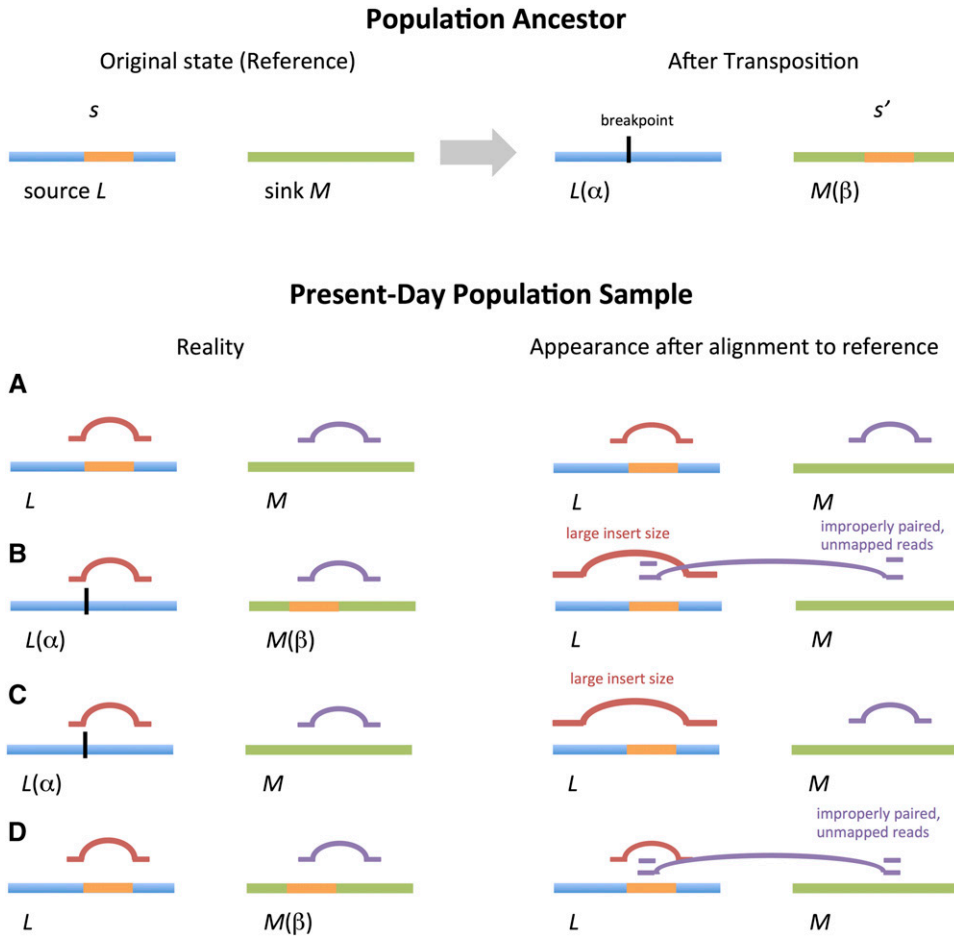


Figure 1 Effects of a transposition on short-read mapping. Chromosomes are horizontal bars and read pairs are pairs of horizontal lines linked by curves. Upper panel: a population ancestor corresponding to the reference genome (left) undergoing a transposition (right), in which a segment s at source locus L with haplotype context α is copied to s' at recipient sink locus M with haplotype context β . Lower panel: all four possible combinations (A–D) of source L and sink M haplotype in descendants. On left are shown the alignment of reads to the true haplotypes, where there are no read-mapping anomalies. On right are shown the read-mapping anomalies that arise, depending on the true haplotype backgrounds at source and sink, upon alignment to the reference genome.

tested by fitting SV trait vectors to the imputed ancestral haplotype at each locus in the 488 genome mosaics. In combination, the mosaics partitioned the genome into 16,700 haplotype blocks, with the ancestral haplotype of all lines unchanged in each one. Let y_{Ai} be the number of anomalous reads of a certain type at source segment A in line i . At every haplotype block p we fitted the linear model:

$$y_{Ai} = \mu_A + \sum_{s \in S} X_{pi}(s) \beta_{Ap}(s) + e_i$$

μ_A is the average trait value at A , $X_{pi}(s)$ is a binary indicator of whether line i carries haplotype s at p , $\beta_{Ap}(s)$ is the effect of founder haplotype s and e_i the error. Founder effects $\beta_{Ap}(s)$ were estimated by ANOVA to test the null hypothesis of no SV-QTL: $H_0(p) : \beta_{Ap}(s) = 0 \quad \forall s$, returning the P -value π_{Ap} for each block p . Let $\lambda_A = \max_p [-\log_{10}(\pi_{Ap})]$ be the genome wide maximum $\log P$ for the scan.

To determine genome-wide statistical significance, controlling for the number of tests and for associations driven by outliers or any non-normality in the SV-traits, we performed 100 permutations T_A of each trait vector y_{Ais} and repeated the genome scan for each one. The distribution of the 100 genome-wide maxima of each of the permutations was used to determine the significance of the observed $\log P$ s of the

original SV-trait. We fitted a parametric generalized extreme value distribution to the permuted maxima (Dudbridge and Koeleman 2004), using the EVD R package to estimate a genome wide corrected $\log P$:

$$\gamma_A = -\log \left\{ 1 - \exp \left[1 + \hat{s}_A \left(\frac{\lambda_A - \hat{a}_A}{\hat{b}_A} \right)^{-(1/\hat{s}_A)} \right] \right\},$$

where \hat{a}_A , \hat{b}_A , and \hat{s}_A are the MLEs of a_A , b_A , and s_A , respectively. This procedure was performed separately for each SV-trait. Study-wide SV-QTL were selected at $FDR < 10^{-2}$, corresponding to $\gamma_A < 10^{-3}$.

Prediction of SV allele frequency

We predicted which founder haplotypes carried a given SV, reasoning they have more anomalous reads compared to those without the SV. For each SV-QTL the founders' contributions were arranged as a 19×19 table, T_{ij} , containing the read anomaly count (of a certain type) at the source for all lines carrying haplotype i at the sink and haplotype j at the source. A founder was classified as carrying the SV if its corresponding row was generally higher than the rest of the table (for *cis* SV-QTL, the matrix is almost diagonal).

The contribution of founder i is defined as $r_i = \sum_j t_{ij}$. We reordered the founders such that $r_1 > \dots > r_{19}$. We reasoned that, if the SV is biallelic with $k \in \{1 \dots 18\}$ founders carrying the SV, then $\sum_{j=1}^k r_j$ would be much larger than expected compared to the null hypothesis of no SV, when $r_1 \approx \dots \approx r_{19}$. The z-score for k is,

$$z_k = \frac{\sum_{j=1}^k r_j - E[r_k]}{\sigma(r_k)},$$

where $E[r_k]$ and $\sigma(r_k)$ are estimated by 1000 permutations of T , denoted as R_{z_k} . We choose k to maximize z_k . We declare k to be significant—and that there is a partitioning of the founders into two groups at the SV—if $<1\%$ of permutations generate a value of z_k exceeding that observed.

Validation of SVs by paired-end data

We used high and low coverage paired-end reads from the 19 founders (Gan *et al.* 2011), and from the MAGIC lines, respectively, to search for enrichment of read pairs linking the source and sink. First, for the high-coverage analysis of the founders, we restricted attention to the 2391 SV-QTL in which we had predicted which founders carried the SV. Using this partitioning, we used Fisher's exact test to compare the numbers of anomalous read pairs (with one read mapped to the source and the other within a variably sized window of $W \in \{5, 20, 30, 40, 50, 100, 150, 200, \text{ and } 400\}$ kb from the sink) in the founders predicted to carry the SV to the other founders. Second, in the low coverage MAGIC data, we performed the same test comparing the 100 lines with the highest read anomaly trait value to the rest of the population.

Validation by de novo contigs

We used BLAT (Kent 2002) to align 5,524,143 short *de novo* assembly contigs (lengths 50–1000 bp) of the 18 nonreference founders to TAIR10 to identify contigs split between the source and sink (where disjoint pieces aligned to each), or shared (where a common piece aligned to both). We excluded genomic regions with annotated repeats or transposons, and alignments that mapped to over five genomic loci. We randomized the SV-QTL by circular genome permutation (Cabrera *et al.* 2012) to determine whether such split and shared contig alignments are overrepresented near SV-QTL. For SV-QTL i , if $u(i), v(i)$ are the original position of the source and sink, respectively, then a permuted SV-QTL $u_k(i), v_k(i)$ is defined as $u_k = (u(i) + \theta_k) \bmod L$, $v_k = (v(i) + \theta_k) \bmod L$, where $\theta_k \sim Unif(0, L)$. We required $u_k(i), v_k(i)$ to be on the same chromosome for *cis* SV-QTL. We then computed one-sided permutation P -values $\pi_{\text{split}}, \pi_{\text{shared}}$.

Validation by PCR

We designed PCR primers for 77 breakpoints from 44 SV-QTL predicted from *de novo* contigs. We conducted 96 *type I* experiments (one for each of the 77 breakpoints) that used

primers corresponding to remote or inverted sink loci, so PCR should produce a product in only in SV genomes and not in the reference. We also performed 19 *type II control* experiments that should produce a PCR product in the reference, but not in SV genomes.

We designed 20–30 bp primer oligos based on the reference (TAIR10), using Primer3 (Rozen and Skaletsky 2000), after masking out repeats, transposons, and known polymorphisms. SVs tend to be near such sequence features, so we relaxed the default Primer3 criteria to detect oligos, and required: (i) Maximum allowed product 1.5 kb, (ii) Annealing temperature 10–90°, (iii) GC-content 10–90%, and (iv) Self-complementarity 8 bp. Primer specificity was tested by BLAT (Kent 2002).

Association with physiological phenotypes

For each of the six read anomaly categories, we computed Pearson correlations and corresponding P -values between nine physiological phenotypes, and the 11,915 SV-traits. We selected significant correlations with $\log P > 4$ (so we expect about one false positive result per scan). After filtering correlations driven by outliers (*i.e.*, in which removal of the three most extreme samples reduced the correlation below the significance threshold), we found 549 SV-traits associated with 40 phenotypes. Each physiological phenotype had, on average, 1.56 associated SV traits of the same anomaly type.

The effect of SVs on each phenotype was measured by a heritability-like measure, h_{SV}^2 , estimated by linear models. Let y be the vector of phenotypic values for a physiological phenotype with k correlated SV traits (of the same type): X_1, \dots, X_k , represented by the matrix X . The phenotype is modeled as:

$$y = Xa + e.$$

The k parameters a were estimated using the R function `glm()`. We also computed the individual effect sizes of SV-traits, by fitting simple linear regression models. We mapped QTL for the phenotype residuals after regressing all/each associated SV traits of the same type, and compared them to the phenotype QTL.

Published phenotypes

We used flowering time and rosette diameter data from a field experiment (Springate and Kover 2014), as well as phenotypes described previously in Kover *et al.* (2009).

Phenotyping resistance

Three replicates of each MAGIC line were grown at the University of Bath in 2.5-inch plastic pots. Plants were monitored daily, and germination and bolting day recorded. After plants senesced, the inflorescence height and the total number of branches were measured. In a separate experiment, MAGIC lines were grown in growth chambers in P24 plastic trays, and sprayed with *A. laibachii* race Nc14 (Thines *et al.* 2009) when

plants were 21 days old. Nc14 zoospores were suspended in water at a concentration of 10^5 spores/ml and incubated on ice for 30 min. The spore suspension was then sprayed on plants using a spray gun, and plants were incubated in a coldroom in the dark overnight. Infected plants were kept in a growth chamber under 10-hr light and 14-hr dark cycles with a 20° day and 16° night temperature (Kemen *et al.* 2011). Resistance was defined as absence of pustules on the leaves at 7 days after inoculation. To minimize errors in scoring, resistant plants were monitored up to 14 days after inoculation. The experiment was reproduced twice.

Collection of RNA

We obtained seeds of MAGIC lines from the Nottingham *Arabidopsis* Stock Centre (NASC) and grew 209 lines at 20° in Percival environmental chambers (Perry, IA), in the laboratory of R.M.C., Salt Lake City. We prepared total RNA from pools of 20 aerial rosettes from seedlings at the fourth true leaf stage (Gan *et al.* 2011). RNAseq library construction and sequencing was performed at the Oxford Genomics Centre (Oxford, UK) to produce 2×100 bp reads using the Illumina nonstrand specific method. Per Illumina HiSeq lane, samples were barcoded and run in 13-plexes to give ~14 million reads per sample.

Alignment of RNAseq reads and expression quantification

All libraries were aligned to the TAIR10 reference gene set augmented by any novel genes reported in Gan *et al.* (2011) using PALMapper v0.6 (Jean *et al.* 2010), following a variation-aware alignment approach. Genome variants collected from the 19 founder strains, as well as variants reported for a diverse natural population (Long *et al.* 2013) were integrated and provided to the aligner as known variants to prevent reference biases in RNAseq read mapping (Gan *et al.* 2011). To facilitate accurate alignments, we provided splice junctions in the founder strains (Gan *et al.* 2011) and from the TAIR10 genome annotation. The full alignment parameter set for PALMapper was: -M 3 -G 0 -E 3 -I 12 -L 14 -K 12 -C 14 -I 5000 -NI 1 -SA 5 -UA 50 -CT 50 -JA 15 -JI 1 -z 10 -S -seed-hit-truncate-threshold 100 -report-map-read -report-spliced-read -report-map-region -report-splice-sites 0.9 -filter-max-mismatches 0 -filter-max-gaps 0 -filter-splice-region 5 -min-spliced-segment-len 1 -qpalma-use-map-max-len 10 -f bam -qpalma-prb-offset-fix -junction-remapping <junction_file> -score-annotated-splice-sites <junction_file> -max-dp-deletions 2 -use-variants-editop-filter -use-variants <variant_file> -filter-variants-minuse 1 -merge-variant-source-ids -use-iupac-snp-variants -filter-variants-map-window 20 -iupac-genome -filter-variants-maxlen 100 -index-precache

Gene expression quantification

We used a custom python script that counted the number of reads overlapping with at least one exonic position of an annotated gene feature. For each read, only the best alignment was considered for counting, and we excluded alignments if the alignment (i) overlapped an annotated

intron, (ii) was entirely in a region where two or more annotated genes overlap, or (iii) did not start at a position inside an exon in all annotated isoforms. For each gene feature, the number of reads passing these filters was used as the expression count.

Effects of SVs on gene expression

We considered only SVs with accurate breakpoints (see section *Validation by de novo contigs*). A total of 119 TAIR10 genes spanned SV breakpoints (*i.e.*, were disrupted by SVs), and 6909 were inside them (transposed, inverted, or duplicated). Genes were divided into three categories: disrupted by breakpoints, within SV-regions, and outside SVs, and compared with respect to mean and variance using *t*-tests. We also computed the correlation of these genes with their local read anomaly values (for the six read anomaly types), *i.e.*, with the 10 kb source region that contains the gene, and compared the mean and variance (by a *t*-test and an *F*-test, respectively) of the Pearson correlation coefficients across categories.

Heritability

We computed genetic relationship matrices K between MAGIC lines three ways:

Identity by descent (haplotype-based) K_H : Each MAGIC chromosome is a mosaic of the 19 founders, which we used to determine identity by descent (IBD). Across N MAGIC lines, we identified the union of all mosaic breakpoints, and then segmented the genome of each MAGIC line according to these breakpoints. Thus, by construction, the founder haplotype for each line is constant within each segment. The founder haplotype in segment L in line i is represented by an indicator matrix H_{if} , which is 1 if the founder is f and 0 otherwise. Then $f_{ijL} = \sum_f H_{if} H_{jf}$ indicates whether lines i, j are IBD at L , and if w_L is the fraction of the genome covered by L , then the fraction of the genome IBD for lines i, j is

$$d_{ij} = \sum_L w_L f_{ijL}.$$

This matrix is then standardized to take the form of a genetic relationship matrix. Let P_L be the probability that, given the observed population-wide founder haplotype fractions at L , two randomly sampled lines are IBD, *i.e.*,

$$P_L = \frac{2 \sum_{i < j} f_{ijL}}{N(N-1)}.$$

Define $E_{ij} = \sum_L w_L (f_{ijL} - P_L)$, $\sigma_i^2 = E_{ii}$, and hence standardize the IBD matrix K_H as

$$K_{Hij} = \frac{\sum_L w_L f_{ijL}}{\sigma_i \sigma_j},$$

which has main diagonal 1, and off diagonal elements in the range $[-1, 1]$. Note that, in a small fraction of cases, $d_{ij} = 0$, and the corresponding values of K_{Hij} all take the same minimum (the horizontal line of points in Figure 8C).

Identity by state (SNP-based) K_S : SNPs were imputed in the MAGIC lines by using the haplotype mosaics and the filtered set of $M = 1.2$ million SNP variants in the 19 founders. If $S_{ip} \in \{0, 1\}$ encodes the homozygous SNP genotype in individual i and SNP p , and, if π_p is the allele frequency at p , then the normalized genotype is

$$T_{ip} = \frac{S_{ip} - \pi_p}{\sqrt{M\pi_p(1 - \pi_p)}},$$

since the MAGIC lines are almost fully inbred the normalization differs slightly from an outbred population under Hardy-Weinberg equilibrium. The SNP-based GRM is the positive semi-definite matrix K_{SNP} , with elements $K_{SNPij} = \sum_p T_{ip}T_{jp}$, or $K_{SNP} = TT'$.

Read Anomalies K_{SV} : We constructed read-anomaly GRMs by analogy to SNP-based GRMs. Let X_{iL} be the read anomaly trait for individual i at locus L . Let $\alpha_L = \sum_i X_{iL}/N$ and $\tau_L^2 = \sum_i X_{iL}^2/N - \alpha_L^2$ be the sample means and variances. Define the standardized trait matrix W with elements

$$W_{iL} = \frac{(X_{iL} - \alpha_L)}{\tau_L \sqrt{M}},$$

where M is the number of loci. The relationship between individuals i, j is $K_{SVij} = \sum_L W_{iL}W_{jL}$, i.e., $K_{SV} = WW'$. We computed a matrix for each of the six measures of read anomaly. The choice of contributing loci was varied as described in the *Results*. In addition, we ignored loci with no anomaly variation, or where only a small fraction ($<3\%$) of individuals varied.

For a phenotype y measured in the MAGIC lines, and a given K matrix, the variance matrix is represented by the mixed model $V(\sigma_g^2, \sigma_e^2) = K\sigma_g^2 + I\sigma_e^2$, where I is the identity matrix, and σ_g^2, σ_e^2 are the genetic and environmental components of variance and the phenotypic heritability is $h^2 = \sigma_g^2/(\sigma_g^2 + \sigma_e^2)$. We estimated heritability by minimizing the negative log-likelihood $-2\log L(\sigma_g^2, \sigma_e^2) = y^T V(\sigma_g^2, \sigma_e^2)^{-1} y + \log |V(\sigma_g^2, \sigma_e^2)|$ with respect to σ_g^2, σ_e^2 , using purpose-written R code based on the eigen-decomposition in (Kang *et al.* 2008a).

Data availability

Source codes and supporting data are available from <http://mtweb.cs.ucl.ac.uk/mus/www/19genomes/magic.html>. MAGIC Genomic short read sequence data are available from ENA under study accession PRJEB19252. MAGIC RNAseq data are available from GEO under series number GSE94107.

Results

Structural variants as quantitative traits

We combined ideas from signature-based SV identification and quantitative genetics to analyze structural variation in a population. The following scenario motivates our reasoning:

suppose an SV arose in a certain population ancestor, α , transposing a genomic segment, s , originating at a “source” locus, L , and targeting to a “sink” locus, M . Source and sink can be coincident or unlinked, but, for the moment, suppose they are unlinked. If the event is transposon-mediated, then the segment s is duplicated to s' at M , and possibly altered, leaving the original s at L . Among the descendent population, random chromosomal assortment and recombination ensures there will be a mix of individuals carrying the segment at neither, one, or both loci.

Among the descendants, one individual is sequenced, and chosen as the reference genome. Depending on the choice of reference individual, and the mechanism of transposition, the reference might carry zero or one copies of s at the source, and of s' at the sink. Assume the reference has one copy of s , and zero copies of s' . In a population sample, only individuals that inherited the haplotype descended from α at the sink carry the transposed segment, regardless of their haplotype at the source. The sample is sequenced with short-reads, and the reads are mapped to the reference genome. Individuals carrying the transposition s' at the sink will have reads spanning the breakpoint that split between source and sink. Hence, read mapping anomalies apparently originating at the source will be enriched in those individuals carrying the sink haplotype α ; genotypes that tag α at the sink will be associated with anomalies at the source.

If, on the other hand, the reference contains both s at the source and s' at the sink, then those individuals that did not inherit the haplotype α at the sink will appear to carry a deletion there. Reads with anomalously large insert sizes will map to the sink, and will be associated with genotypes tagging the haplotype α at the sink—the generative role played by the source will be invisible.

Similarly, by considering other situations—for example, tandem duplications—where the source and sink are coincident in a population, we would expect to encounter a mix of short-range *cis* and long-range *trans* associations between various classes of read-mapping anomalies and genotypes, depending on the history of each structural variant.

To apply these ideas in practice, we count the numbers of anomalous reads mapping to each source L in a population sample, treat it as a quantitative trait, and identify genetic loci whose genotypes correlate with variation in the SV-trait. This defines an SV-QTL associating T_{Li} , the number of anomalous reads mapping to locus L in individual i , and the haplotype H_{Mi} at sink locus M in individual i (Figure 1 and *Materials and Methods*). *cis* SV-QTL are where the source and sink overlap and indicate local structural variants such as CNVs, deletions and inversions; *trans* SV-QTL indicate transpositions (insertional translocations) or larger scale rearrangements. In this way, we may determine whether an SV is in *trans*, its originating haplotype, which individuals now carry it (Supplemental Material, Figure S1), and its frequency (Figure S2).

Structural variation in *Arabidopsis*

We used our strategy to map SVs in the 120 Mb genome of the plant *A. thaliana*. We sequenced 488 of the *Arabidopsis* MAGIC recombinant inbred lines (Kover *et al.* 2009) at $\sim 0.3\times$ coverage using 51 bp paired-end Illumina reads. The MAGIC lines descend from 19 ancestral founder accessions that have been previously sequenced at high coverage (Gan *et al.* 2011) (Table S1), such that each MAGIC chromosome is a mosaic of the 19 founder haplotypes. Consequently, we expect most SVs segregating in MAGIC to also segregate in the founders, thereby providing a means of verifying any SVs we detect. The choice of MAGIC lines rather than natural accessions means that the confounding effects of population structure, and of selection, are largely absent from the population. Very rare alleles with frequency below $1/19 = 4.5\%$ are uncommon, increasing the power to detect QTL. However, MAGIC QTL mapping resolution is also poorer, at ~ 200 kb, compared to ~ 10 kb in natural accessions.

We mapped the reads to the TAIR10 reference using Stampy (Li and Durbin 2010; Lunter and Goodson 2011), and inferred the mosaic of each line using a hidden Markov model (HMM) implemented in the software “reconstruction” available from <http://mtweb.cs.ucl.ac.uk/mus/www/19genomes/magic.html>. The algorithm uses as input SNP calls for each MAGIC genome, and 1.2 M biallelic variants segregating in the 19 founders (excluding loci tagged as within transposons, and those sites called as heterozygous or multi-allelic in the founders) (Gan *et al.* 2011), and finds the most likely sequence of haplotype assignments for each chromosome. Because the lines were called at low coverage, most SNP sites were not covered by reads in any given line; consequently we called on average 301k SNPs per line (using GATK; McKenna *et al.* 2010) (*i.e.*, a randomly sampled of $\sim 25\%$ of the 1.2 M sites). However, these data are sufficient for the HMM to determine the founder mosaic accurately; we estimated by simulation that mosaic breakpoints (which correspond to recombination events) were mapped to within ~ 2 kb (data not shown).

Using this procedure, we reconstructed each MAGIC genome into ~ 34 haplotype blocks, on average, with mean size 3.48 Mb, representing contributions from ~ 11 founder haplotypes (Table S2). We imputed the full variant catalog into each line. Comparison of imputed SNPs with 782 GoldenGate SNP genotypes measured in 370 of the MAGIC lines (Kover *et al.* 2009) showed 98% concordance.

To map SVs, we divided the reference genome into 11,915 abutting source loci, each 10 kb wide, and computed six measures of anomalous read mapping in each locus ($6 \times 11,915 = 71,490$ SV trait vectors) (Materials and Methods, Table 1). Four of these measures address different types of anomalous read mapping, diagnostic of specific anomalies, namely high read coverage for duplications, strandedness of reads for inversions, anomalously large insert size for translocations, and unpaired reads for deletions.

The remaining two measures are linear combinations of other measures.

Genetic association between each of the SV-trait vectors and the local haplotype space was determined using a one-way ANOVA. We chose to determine association at the level of haplotypes rather than SNPs for two reasons. First, the founder haplotype space in the MAGIC lines is well-defined, and measuring association with haplotypes can capture relationships invisible at the level of SNPs. Second, the set of haplotype tests—defined by the union of all the breakpoints across the lines, comprising 16,700 haplotype blocks, such that the ancestral haplotype of all lines is unchanged within each block—means $\sim 75\times$ fewer tests are performed, thereby speeding up the procedure (Materials and Methods). To determine genome-wide significance thresholds for SV-QTL, we performed 100 phenotype permutations for each trait, and then fitted extreme value distributions (evd) to the genome-wide maxima of the permutations (Dudbridge and Koeleman 2004) (Materials and Methods).

At this 1% FDR (evd $P < 0.001$), we mapped 10,275 SV-QTL in total. Table S3 shows mapped QTL per read anomaly category; 3773 SV-QTL had coincident sources and sinks, probably corresponding to the same SV, and were merged, leaving 6502 SV-QTL, tabulated in Table S4. Of these, 1604 (25%) were *trans*, defined as mapping >2 Mb from the source. Overall, 4073/11,915 (34.2%) source loci harbored structural variants. While we have greater power to detect larger SVs, 2379 overlapped annotated indels <2 kb (Gan *et al.* 2011).

The likelihood that a structural trait vector has an SV-QTL increases with its variance (Figure 2). SV-QTL are enriched around centromeres, as expected. Away from the centromeres, Figure 2 also shows that bins with variable SV traits are isolated, rather than in clusters. Figure 3A shows the genome-wide distribution of SV-QTL segregating in one MAGIC founder, Ler-0. Figure 3 and Table S3 show that *trans* SV-QTL link all five chromosomes.

In 319 SVs, we were able to pinpoint both breakpoints exactly (see Validation) Mean SV size was 53 kb in these SVs, and the largest was 189 kb. Thus, many of the SVs we discovered are too large to be due to insertions of small transposable elements. This probably reflects our lack of power to detect very small events, but also emphasizes that not all SVs are driven by mobile elements.

Validation

Genome-wide confirmation of SVs using short-read sequence is challenging because SV breakpoints often associate with transposons and repeats that hinder read-mapping and reassembly. However, among our SV-QTL are several known rearrangements. These include *trans* SV-QTL linking a cluster of rDNA repeats at ~ 14.2 Mb on chromosome 3, to clusters at the ends of chromosome 2. Polymorphisms in these clusters are implicated in massive genome size variations among *Arabidopsis* accessions (Long *et al.* 2013; Rabanal *et al.* 2016). We also identified the known knob inversion on

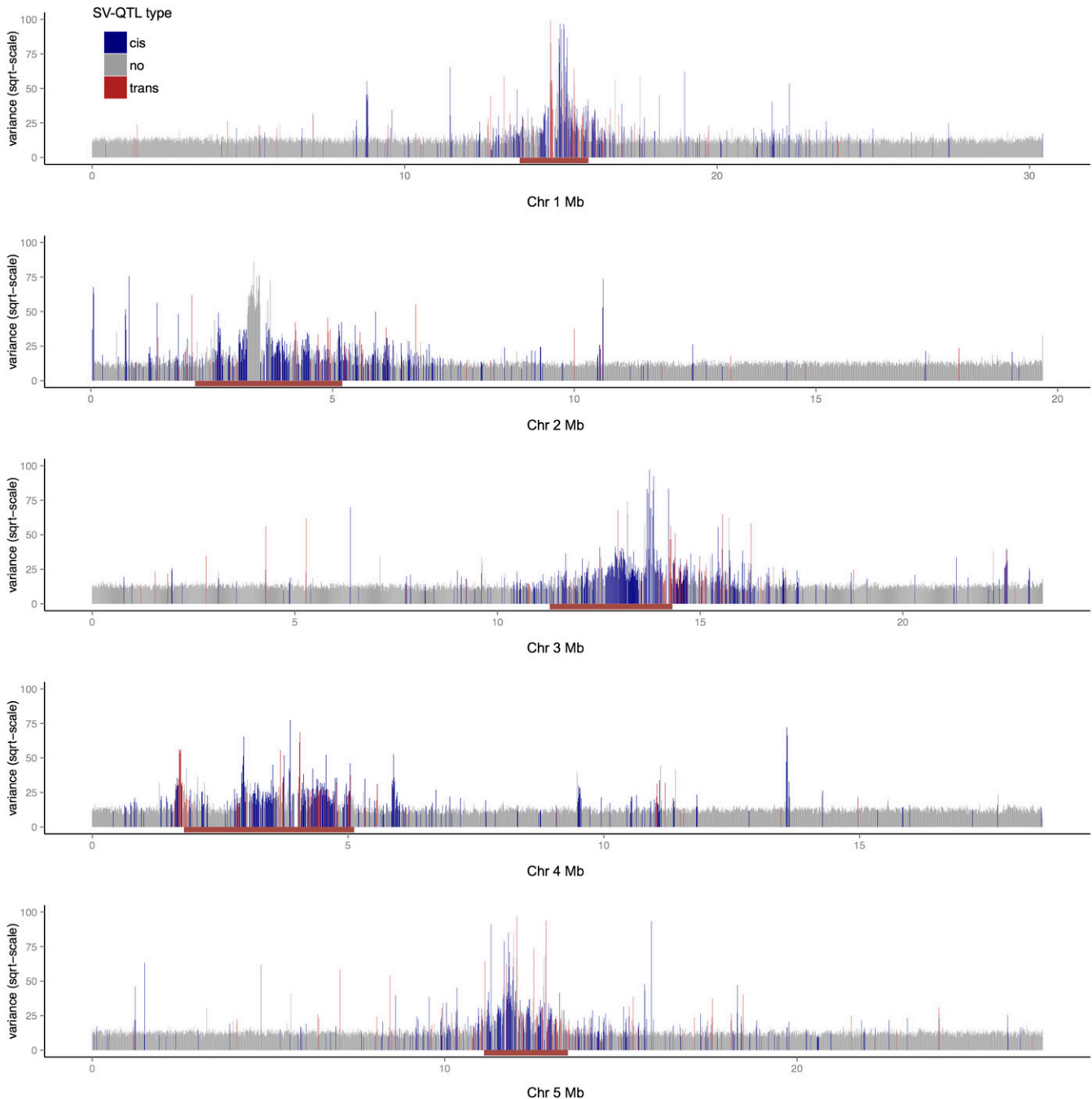


Figure 2 Genome-wide distribution of the variance for the trait “improperly paired reads,” computed in 10-kb windows. The x-axis shows genomic position and the y-axis the variance of each trait vector scaled by its mean. Each vertical line corresponds to a window; those with SV-QTL are blue (*cis*) and red (*trans*). The centromeres are marked by brown horizontal bars.

chromosome 4 as reciprocal transpositions linking 1.61 and 2.65 Mb (Fransz *et al.* 2000), and a 93 kb inverted transposition identified previously in a cross between Ler-0 and Col-0 (Wijnker *et al.* 2013), and found it was present in 12 MAGIC founders.

To validate further SVs, we compared our SV calls for the founder accession Ler-0 against two Ler-0 contigs (chr3:16.65–17.02 Mb, chr5:25.06–25.23 Mb) that were independently resequenced and manually reassembled (Lai

et al. 2011), thereby constituting a gold standard for comparison. The chromosome 3 contig (Figure 4) is enriched in SVs (83 indels, 31 > 100 bp), consistent with our analysis: 42 SV-QTL sources (36 *cis* and six *trans*) are in this region, and four *trans* SV-QTL map into it. As would be expected, the sources of these SV-QTL are within gaps in the contig. Furthermore, alignment revealed two long-range SVs within the contig (a transposition and a duplication that align to chromosomes 4 and 2, respectively), which coincide with the

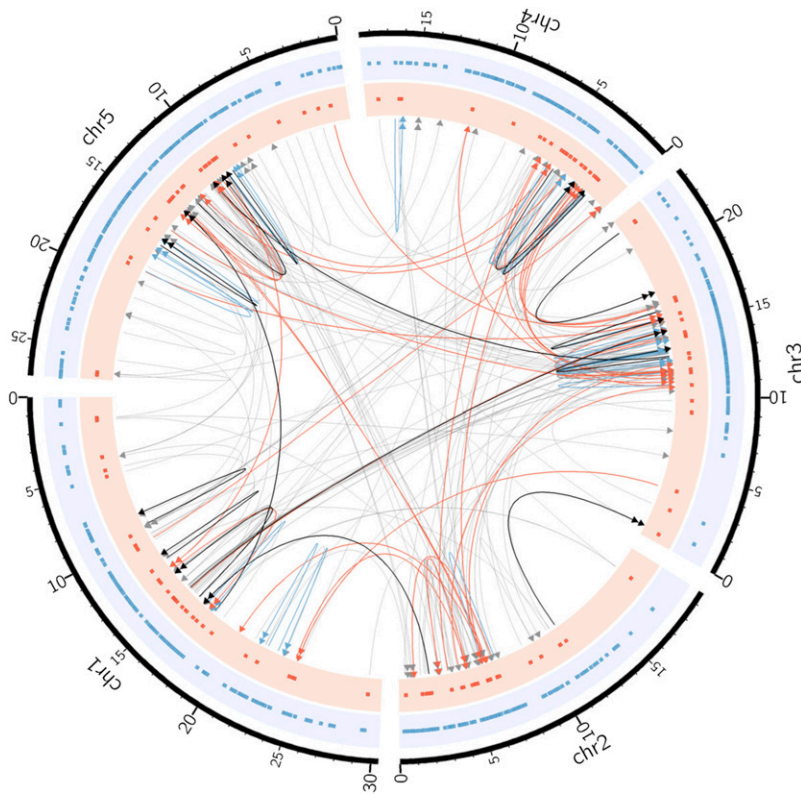


Figure 3 Structural variants segregating in the accession Ler-0. The gray directed lines show SV-QTL, with the arrows pointing toward the sink locus. Red and blue links indicate 37 *trans* and 30 *cis* SV-QTL, confirmed by *de novo* contigs. The black links show 16 SVs confirmed by PCR (seven *cis*, nine *trans*). Double arrows in links indicate inversions. The dots in the red and blue tracks mark the sources (*trans* and *cis*, respectively) of all SVs associated with the Ler-0 haplotype.

source and sink of two *trans* SV-QTL mapped within the contig. Similarly, in the chromosome 5 contig, six *cis* SV-QTL correspond to deletions (Figure S3).

We also analyzed an independent *de novo* assembly of Ler-0 built from long PAC-BIO reads, GenBank accession GCA_000835945.1 (Berlin *et al.* 2015) to validate our *trans* SV predictions. This assembly was constructed algorithmically without manual revisions, and so is not guaranteed to be correct. Further, the Ler-0 individual sequenced in the PAC-BIO assembly was different from the individual that founded the MAGIC population, and therefore might carry private structural variations. Nonetheless, we expect it to be more accurate and contiguous than a Ler-0 assembly built from short Illumina reads alone. We took those 3080 Illumina paired-end reads for Ler-0 from Gan *et al.* (2011) that carried large insert size mapping anomalies when mapped to TAIR10, and that mapped to the sources of our predicted Ler-0 *trans* SV-QTL, and then mapped them to the PAC-BIO assembly using BWA (Li and Durbin 2010). These Illumina reads are from an individual grown from the same batch of seeds used to found the MAGIC population in ~2007, and should therefore share the same structural variants. Read anomalies with correct SV predictions should map contiguously to the PAC-BIO assembly, if the latter assembly accurately portrays the Ler-0 genome. We found 2460 (80%) of these formerly split Illumina read pairs now mapped contiguously, defined as both members of a read-pair mapping to the PAC-BIO assembly with an insert size below 600 bp.

With the exception of these manually assembled Ler-0 contigs, and the provisional Ler-0 PAC-BIO assembly, the MAGIC founders are not contiguously reassembled into a genome-wide gold standard reference panel. Nevertheless, they provide information to test our predictions: at each SV-QTL, we predicted which founder haplotypes carried SVs at the origination of the population, under the assumption the SV was biallelic. Using the low coverage data for the 488 MAGIC lines, at each SV-QTL, we then predicted which founders carried the SV allele, based on correspondence between their SV-trait value and predicted founder allele, using the fact that SV haplotypes have elevated anomalous reads. We did this confidently at 2391 SVs where the founders partitioned into two groups, the remainder having complex multi-allelic SV predictions (*Materials and Methods*). Examples of founder partitions for *cis* and *trans* SV-QTL are shown in Figure S1.

We then examined the independently collected high-coverage reads in each of the 19 MAGIC founders (Gan *et al.* 2011) for read-mapping signatures that supported the predicted grouping of founders at each SV. We counted the read pairs linking source and sink at each of the 2391 SVs in the 19 high coverage founders. At 1585/2391 (66.3%, FDR 7.5%) SVs, we observed significant differences in anomalies between the predicted groupings of founders (Figure S4, which also shows that the majority of SVs were mapped within 50 kb). In the founders, the mean SV allele frequency was $6/19 = 31\%$. Only 387 (12%) were private to a single founder (Figure S2), in contrast to the fraction of SNPs (45%)

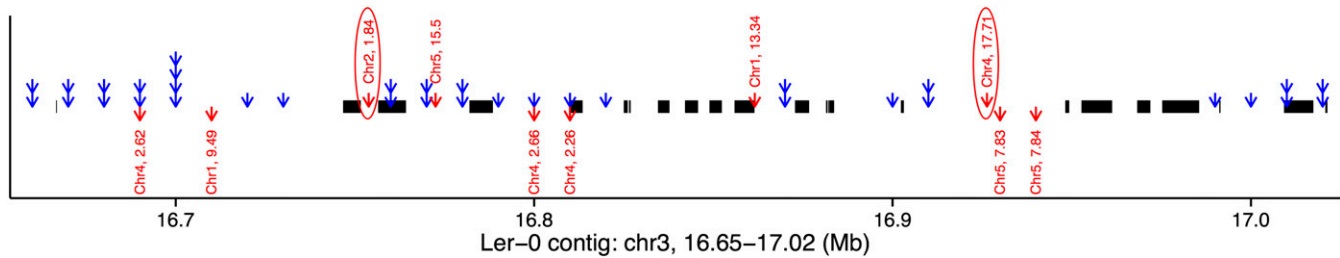


Figure 4 Alignment of a manually assembled contig from Ler-0, chr3:16.65–17.02 Mb to the reference annotated with SV-QTL. Thick black lines show alignments to reference genome. Blue arrows show the sources of *cis* SV-QTL; stacked arrows mean multiple read anomaly traits had SV-QTL. Red arrows display *trans* QTL with arrows starting from the source, and pointing toward the sink. Gaps in the contig alignment indicate loci where Ler-0 did not align to the reference, with the exception of two transposed segments that mapped to chromosomes 2 and 4 at positions concordant with the sources of two *trans* SV-QTL (circled).

that are private to a single founder (Gan *et al.* 2011). This may reflect our lack of power to detect private SVs.

Independent analysis of low-coverage reads from the 488 MAGIC genomes (*Materials and Methods*) supported 1228/2391 (51.3%, most also supported by the founder genomes) and 1631/4111 (39.7%) of those remaining SVs without founder predictions. In total, 2965/6502 (45.6%) SVs were supported by either method.

Breakpoint prediction and confirmation

To estimate SV sizes and identify SV breakpoints to test by PCR, we next *de novo* assembled the high-coverage sequence data for the MAGIC founders into high-quality short contigs, each up to a few kilobases long. We aligned these contigs to the reference to find alignments split between sources and sinks. We found 2619 contigs with alignments split into disjoint pieces across 420 QTL sources and sinks, suggesting a cut-and-paste mechanism (*Materials and Methods*, and Table S4). Of these, at 319 SV-QTL both breakpoints were identified. We found 460,656 (8.3%) shared contigs whose alignments overlapped between source and sink regions.

We designed PCR primers at 77 breakpoints from 45 predicted SVs (both breakpoints in seven SVs, and one in each of the remaining 38). In 30 (66.6%) SVs, 46 *type 1* experiments (designed to amplify in the presence of the predicted SV but not the reference, *Materials and Methods*), at least one breakpoint was confirmed, *i.e.*, there was at least one *type 1* experiment that amplified in founders predicted to carry the SV, while not producing a product in the reference, as expected. In a further seven SV-QTL (15.6%) (15 *type 1* experiments) the founders carrying an SV-QTL were amplified, but, unexpectedly, the reference genome was also amplified. This suggests the presence of duplicated sequence nearby, causing unexpected binding of one of the primers. It might also indicate errors in the reference assembly. In 10/15 cases, we observed duplications (multiple PCR bands) in >2 founders. However, in all 15 cases at least three founder genomes amplified differently from the reference, indicating that the locus is structurally variant, but not exactly as predicted. The remaining 16 *type 1* experiments failed to amplify in any founder. Of the 19 *type 2* experiments (designed to amplify

in the presence of the reference but not the SV), 16 amplified as expected, two were ambiguous, and one failed.

Overall, we confirmed at least 30 (66.6%) SVs at either or both breakpoints, and, at a further 7 (15.6%), we found evidence of structural variation. Among the total of 37 SVs supported by PCR, we confirmed 61 (79%) breakpoints. There were 14 *cis* (six inversions, seven transpositions, and one indel) and 23 *trans* (13 with inversions) SV-QTL (Table S5). Consistent with our difficulties in predicting biallelic founder alleles, in 11 SVs, the breakpoints were polymorphic among the founders carrying the SV, and, in five transpositions, the orientation of the SV differed between founders.

Effects of SVs on phenotypic QTL and gene expression

We next investigated associations between SVs and nine physiological phenotypes, either previously published (Kover *et al.* 2009; Springate and Kover 2014), or first reported in this study (Table S6). We found 16 distinct SV-QTL (eight in *trans*, Table S7) that overlap physiological QTL. In some cases, regressing the SV-trait from the physiological trait ablated the physiological QTL, consistent with, albeit not proving, that the SV is causal. This is illustrated by a QTL for germination time (Kover *et al.* 2009) on chromosome 3, which is ablated by a *cis* SV-QTL for unpaired reads at ~15,936,650–15,951,640 bp (Figure 5, A and B). Our analysis predicts seven founders carry a deletion at this locus, which was confirmed by the independent founder sequences (Figure 5C), revealing a 15 kb deletion containing three genes, AT3G44240 (Polynucleotidyl transferase, ribonuclease H-like superfamily protein), AT3G44245 (pseudogene of cytochrome P450, family 71, subfamily B, polypeptide 21), and CYP71B38 (AT3G44250, cytochrome P450, family 71, subfamily B, polypeptide 38). Other SVs segregate nearby, but with allelic patterns inconsistent with the trait, and therefore unlikely to be causal. It is probable that the deletion contains the causal variant(s). The deleted genes are not known to affect germination, although a mutant of another polynucleotidyl transferase, *AHG2* (AT1G55870) does (Nishimura *et al.* 2009).

We found similar effects on the chromosome 4 QTL for resistance to the fungal pathogen *A. laibachii*, isolate Nc14

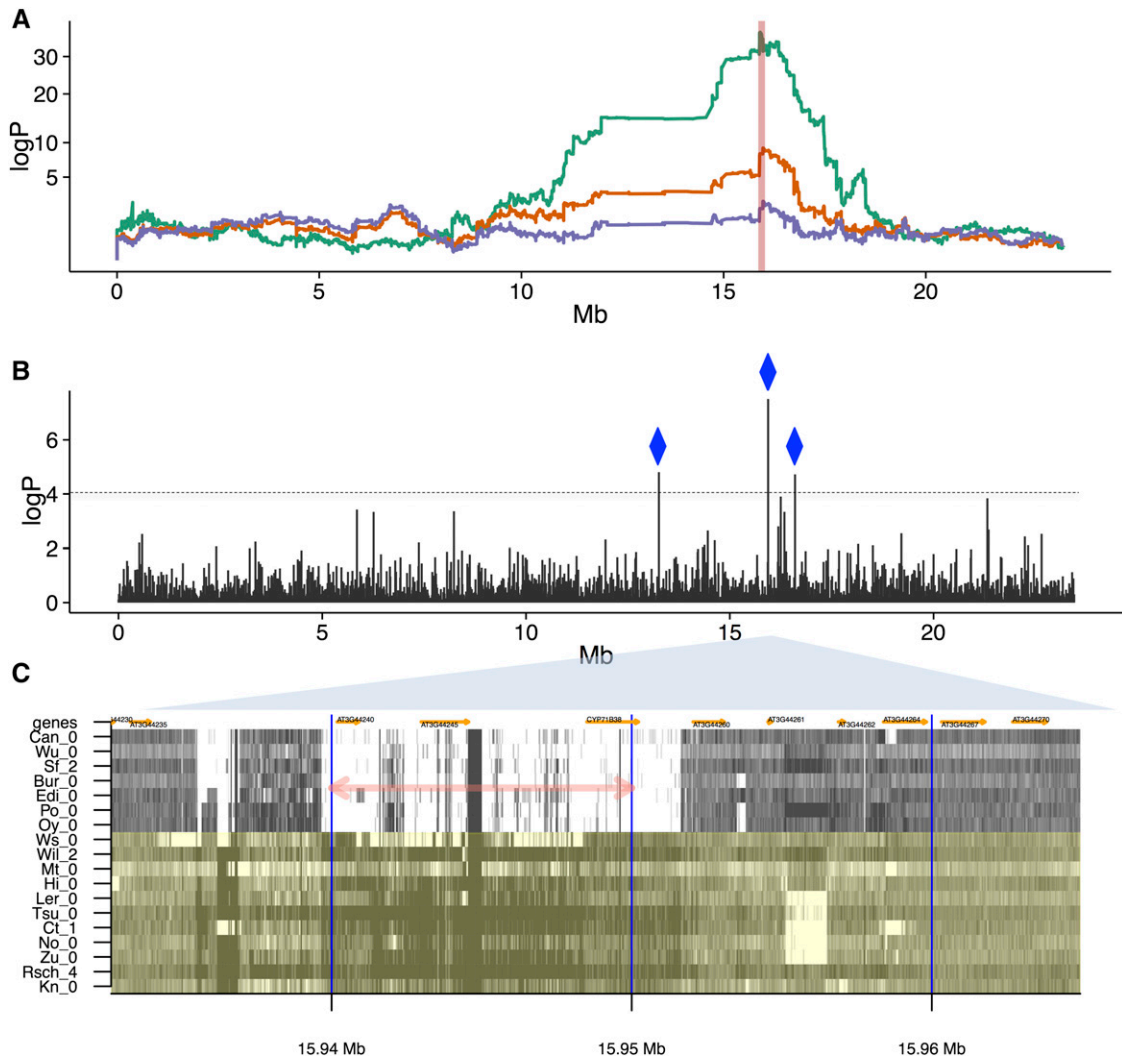


Figure 5 Effects of SVs on germination time. (A) Genome scans over chromosome 3 (x-axis: genomic position, y-axis: $\log P$ of association). Orange: association of local haplotype with germination time (days), peaking at 15.93 Mb. Green: association of local haplotype with the SV trait unpaired reads at the source locus 15.94–15.95 Mb (indicated by the vertical red line), explaining 8.13% of the variance in germination time, with an SV-QTL mapped at the same position as the germination QTL. Purple: residuals of germination time after regressing out the SV trait, ablating the QTL. (B) Chromosome-wide Pearson correlations between germination time and the numbers of unpaired reads measured at each 10 kb source locus (x-axis: genomic position, y-axis: $-\log_{10}$ P -value of test that the correlation is zero). Three source loci correlate strongly with germination ($\log P > 4$), all with *cis* SV-QTL (blue diamonds). (C) Structural variation in the MAGIC founders. Shown is the read coverage in 18 accessions (labeled on y-axis), covering ~30 kb surrounding ~15.94 Mb (x-axis). Dark shades indicate high coverage, light shades low coverage. The 10 kb intervals used to define source loci are delineated by vertical blue lines. The source locus giving rise to the SV-QTL in (A), (B) is marked with a pink double-arrow. Those founder accessions predicted to carry the reference allele (No-0, Ct-1, Mt-0, Wil-2, Ler-0, Tsu-0, Rsch-4, Kn-0, Zu-0, Hi-0, and Ws-0) are in green, those predicted to carry the SV are in gray. Genes are annotated in orange.

(Thines *et al.* 2009) (Figure 6 and Table S7). Variation in the number of unpaired reads at 9.50–9.51 Mb explains 18.3% of the variance in resistance, and is adjacent to a cluster of leucine-rich repeat genes, and the genes *RPP4* (Van Der Biezen *et al.* 2002), *BAL* (Yi and Richards 2009), and *RPP5*. This locus is rearranged in some *Arabidopsis* accessions, and is known to affect disease resistance (Yi and Richards 2009); Figure 6 confirms the founder genomes have complex, polymorphic, SVs in this region. Since the resistance QTL is not completely ablated by the SV traits associated with it, additional nonstructural variants likely contribute to it.

Importantly, Figure 5B and Figure 6B show that correlations between SV traits and phenotypes are tightly localized, generally within the width of a single SV trait window, in contrast with wider linkage disequilibrium decay seen in QTL genetic mapping (Figure 5A). Therefore, correlations between SV traits and physiological traits pinpoint causal variants within physiological QTL that are otherwise too broad to localize [mapping resolution in MAGIC is ~200 kb (Kover *et al.* 2009)].

We also corroborated studies (Yalcin *et al.* 2011; Quadraña *et al.* 2016) showing SVs associate with gene dysregulation,

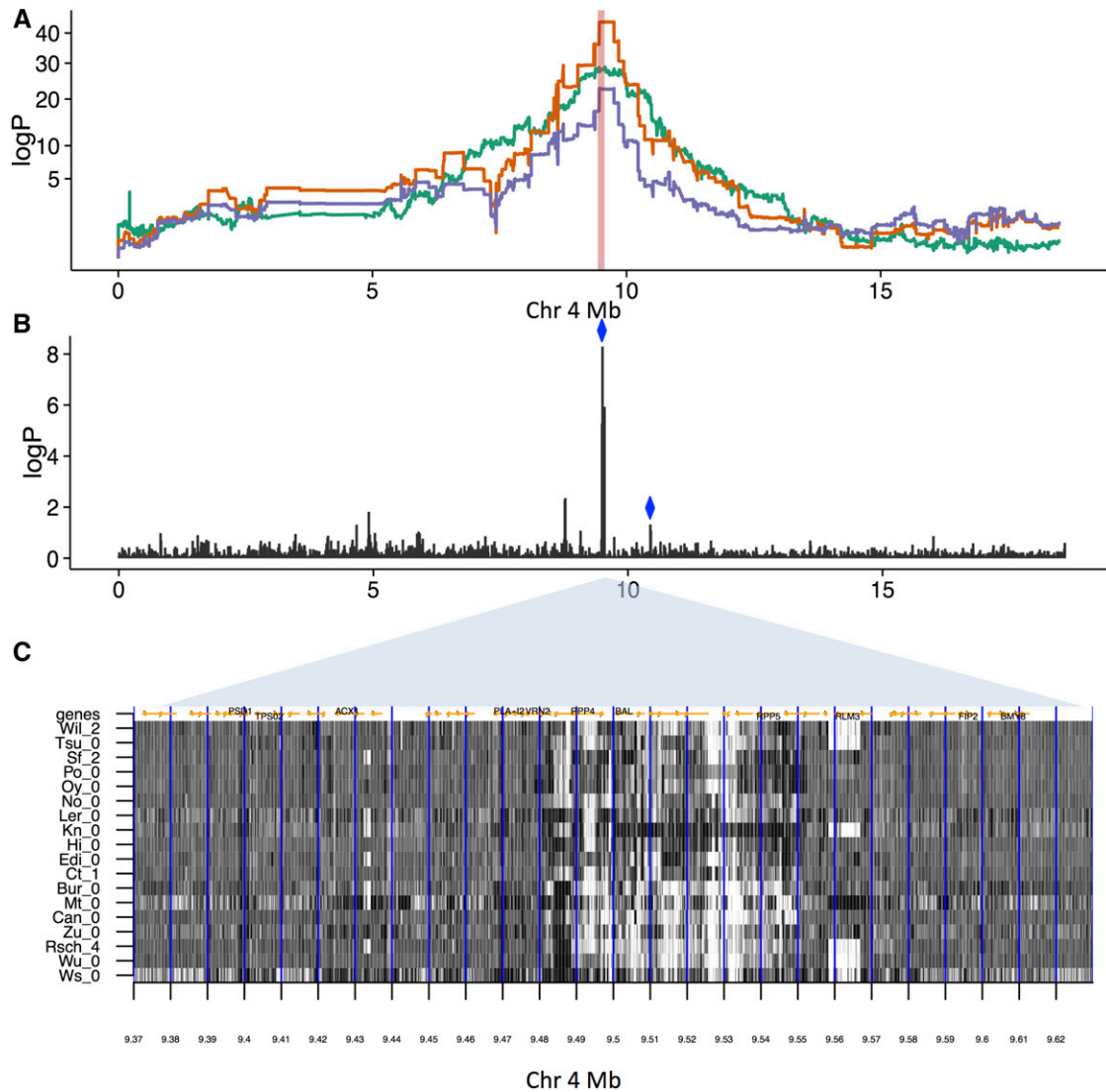


Figure 6 Effects of SVs on resistance to *Albugo laibachii* infection, (A) Genome scans on chromosome 4. Orange: Association with resistance. The peak of association for is at 9.50 Mb. Green: Association with SV-trait improperly paired reads at source 9.50–9.51. Purple: Resistance after two SV traits have been regressed out measuring improperly paired reads [sources chr4, 9.50–9.51 Mb (green line) and chr4, 10.44–10.45 Mb (not shown), both marked with blue diamonds in (B)] that together explain 24.7% of the phenotypic variance. (B) $\log P$ of association between SV traits for improperly paired reads and the resistance trait. There is a cluster of associated traits near 9.50 Mb, in addition to the more weakly associated trait at 10.44–10.45 Mb. (C) Structural variation in high-coverage sequence in the MAGIC founders ~ 9.50 Mb. Shown is the number of improperly paired reads (dark: high values, light: low values) in 18 accessions (labeled on y-axis), between 9.37 and 9.63 Mb (x-axis). The 10 kb intervals used to define source loci are delineated by vertical blue lines. There is a region of complex structural variation spanning ~ 9.48 – 9.55 Mb, with considerable variation between the founder accessions. Genes are marked by orange arrows, and selected genes, some implicated in disease resistance at this locus, are labeled.

even when the gene sequence is undisturbed. Within those SVs with mapped breakpoints, 119 genes spanned the breakpoints, 6909 lay inside the SVs (Table S8), and 21,747 outside. Using RNA-seq from 200 MAGIC aerial seedlings, scaled expression variance increased among genes spanning breakpoints (t -test: $P < 9 \times 10^{-3}$) and within SVs ($P < 1 \times 10^{-13}$) (Figure 7A). Similarly, more lines exhibited silenced transcripts for genes spanning breakpoints (t -test $P < 1.2 \times 10^{-2}$), or within SVs ($P < 2 \times 10^{-52}$) (Figure 7B). Expression within SVs was more correlated with local SV traits than outside SVs (F -test $P < 2.1 \times 10^{-6}$) (Figure 7C).

Effects of SV-traits on heritability

Finally, we treated the SV traits as if they were quantitative, noisy genotypes, to compute pairwise correlations between MAGIC lines, as weighted correlations of their SV traits (Materials and Methods). We constructed SV genetic relationship matrices (GRMs) K_{SV} , which we used to compute the SV-heritability h_{SV}^2 of each of the physiological traits mapped above by analogy with the mixed models used for estimating SNP-based heritability (Kang *et al.* 2008a). This idea resembles the use of gene expression data to model intersample relationships (Kang *et al.* 2008b). We also compared these

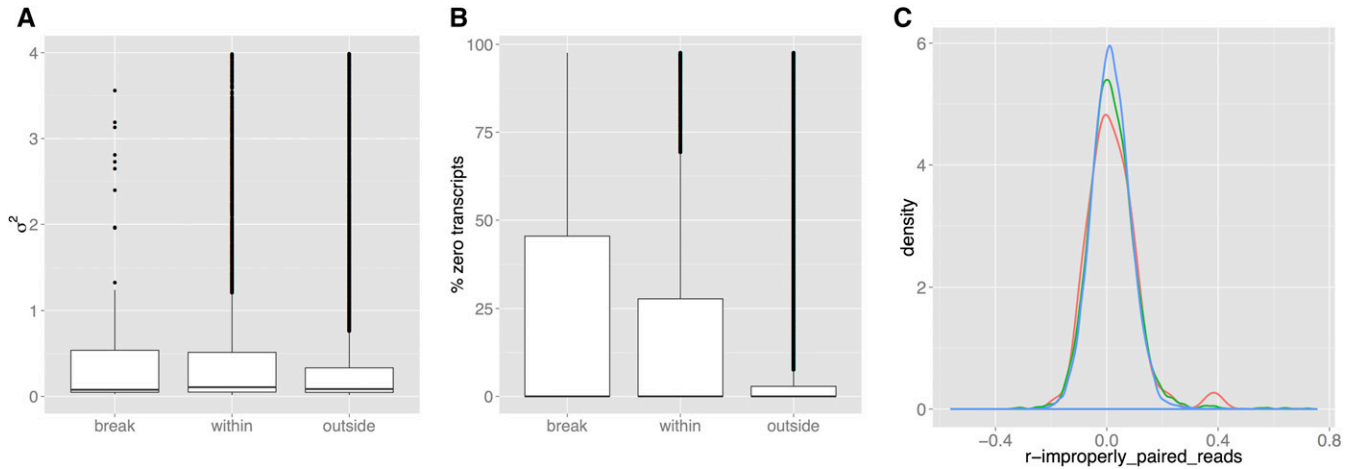


Figure 7 Variation of expression in 200 MAGIC leaf transcriptomes, in genes spanning SV breakpoints, within SVs or outside SVs. (A) Boxplots of transcript variance (scaled by the mean). (B) Boxplots of the fractions of silenced genes (C) Distributions of the Pearson correlations between gene expression and number of improperly-paired reads in the locus containing the gene (red: spanning breakpoints, green: within SVs, blue: outside SVs).

SV-heritabilities with those obtained from “classical” haplotype K_H or SNP-based K_{SNP} GRMs (Table 2). K_H was computed from the identity between haplotype mosaics (*i.e.*, IBD), while K_{SNP} and K_{SV} were computed from the correlations of 1.2 M imputed SNPs or 12k SV-traits, respectively (*Materials and Methods*). We also computed SV heritability when only the most variable 50 or 25% of SV-traits were included, to test if heritability was concentrated at the most structurally variable loci.

As expected, SNP-based heritability h_{SNP}^2 resembles haplotype-based heritability h_H^2 for all phenotypes tested. However, the her-

itability h_{SV}^2 captured by the six measures of SV anomaly is more variable, sometimes being close to zero, but sometimes exceeding classical heritability considerably (Table 2). The SE of h_{SV}^2 was typically about twice that of h_{SNP}^2 or h_H^2 , (~ 0.1 compared to 0.05), presumably reflecting greater uncertainty in SV-traits. Therefore the larger h_{SV}^2 estimates should be treated with caution. Nonetheless, for phenotypes such as time to germination or bolting, the SEs of all estimates are ~ 0.05 , and it is possible to compare them. Figure 8, A and B illustrates likelihood curves for the times to germination (A) and bolting (B), for SNP, haplotype and large insert-size anomalies. Visualizing the entire curves gives a

Table 2 Estimates of heritability

Phenotype	h_H^2	h_{SNP}^2	h_{SV}^2				
			IP	LIS	SS	U	U + LIS
Resistance (resistance to <i>A. laibachii</i>)	0.000 (0.139)	0.258 (0.085)	0.490 (0.335)	0.511 (0.307)	0.000 (NA)	0.673 (0.504)	0.503 (0.314)
RosetteLeafNumber.LongDay (number of leaves in a rosette for plants grown under long daylight)	0.228 (0.081)	0.322 (0.076)	0.463 (0.148)	0.456 (0.146)	1.000 (NA)	1.000 (0.377)	0.447 (0.146)
RosetteLeafNumber.ShortDay (number of leaves in a rosette for plants grown under short daylight)	0.038 (0.060)	0.047 (0.062)	0.000 (NA)	0.000 (NA)	0.000 (NA)	0.000 (NA)	0.000 (NA)
Bolting.Bath (bolting time in a greenhouse)	0.426 (0.064)	0.476 (0.048)	0.783 (0.093)	0.783 (0.093)	0.952 (0.047)	0.989 (0.025)	0.785 (0.092)
Days.to.germ. (germination time)	0.220 (0.068)	0.149 (0.063)	0.385 (0.116)	0.357 (0.113)	0.598 (0.165)	0.835 (0.146)	0.365 (0.114)
FieldFT.pl (flowering time in the field)	0.000 (0.068)	0.095 (0.076)	0.000 (0.179)	0.000 (0.130)	0.000 (0.913)	0.000 (NA)	0.000 (0.145)
FieldRD.pl (rosette diameter plasticity)	0.000 (NA)	0.000 (0.063)	0.000 (0.085)	0.000 (0.084)	0.000 (0.239)	0.166 (0.220)	0.000 (0.085)
Leaves.day.28.given.days.to.germ (residuals for number of leaves at day 28 regressed on germination)	0.193 (0.081)	0.299 (0.066)	0.391 (0.146)	0.362 (0.140)	0.836 (0.189)	0.675 (0.272)	0.366 (0.142)
ttl_branch.BATH (total number of branches of plants)	0.106 (0.048)	0.196 (0.054)	0.276 (0.104)	0.275 (0.100)	0.419 (0.193)	0.616 (0.214)	0.279 (0.102)

h_H^2 is haplotype-based heritability. h_{SNP}^2 is SNP-based heritability. h_{SV}^2 is the heritability estimated from structural variant anomaly traits. Numbers in brackets are the standard errors (SEs) of the heritability estimates above. Heritability for excess reads are not reported because the fraction of bins in any individual containing nonzero entries was too small. IP, Improperly-paired; LIS, Large Insert Size; SS, Same Strand; U, Unpaired; U + LIS, Unpaired or Large Insert Size.

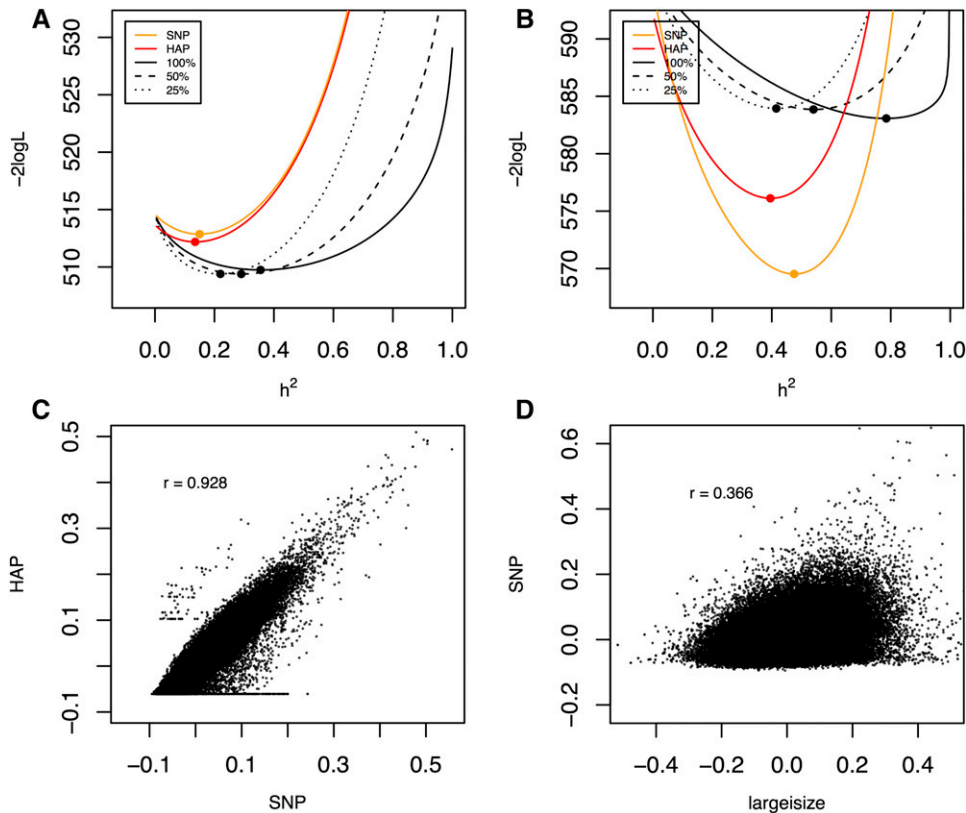


Figure 8 (A, B) log-likelihood curves for two phenotypes Days.to.germ and Bolting.Bath (both with large insert size anomalies), illustrating contrasting behavior of heritability estimates based on structural variants, SNPs, and haplotypes. Log-likelihood curves as functions of heritability are plotted for the GRMs estimated from SNPs, haplotypes, and various fractions of anomalies. The maximum likelihood estimates of each heritability measure correspond to the minima of the corresponding curves, and are marked with dots. (C, D) Scatter plots comparing the off-diagonal elements of genetic relationship matrices. (C) K_{SNP} vs. K_{H} ; (D) K_{SNP} vs. $K_{\text{largeinsert}}$.

better sense of the uncertainty of the maximum likelihood estimates at the curves' minima (the SEs in Table 2 are asymptotic estimates based on the curvature at these minima). Figure 8B shows that, for bolting time, the heritability attributable to all largeinsert SV-traits, $h^2_{\text{largeinsert}}$, is close to 80%, compared to 40–50% for haplotype or SNP-based estimates. As the fraction of SV traits is reduced by progressively removing those traits with lower variance, $h^2_{\text{largeinsert}}$ reduces to that of SNPs or haplotypes. This suggests that there is genome-wide structural variation that is not tagged by standard genetic variation, and which has important effects on specific phenotypes. These effects are not universal, as Figure 8A shows for germination time, where heritability is similar for all GRMs.

The independence of the heritability estimates is borne out by low correlations between the corresponding elements of SNP and SV-based GRMs, which range ~ 0.3 depending on the anomaly type (Figure 8D shows the relationship between GRMs computed from SNPs vs. large insert size anomalies), compared to the correlation of 0.93 between SNP and haplotype based GRMs (Figure 8C).

Discussion

We have combined analysis of the read-mapping signatures commonly used to detect SVs in individuals sequenced at high coverage, with association mapping in populations (Durkin *et al.* 2012). Related ideas based on linkage disequilibrium have been used for mapping unlocalized contigs into reference assemblies (Genovese *et al.* 2013). In doing so, we have

generated a partial catalog of SVs in *Arabidopsis*, although our purpose is not to call SVs systematically, a task that remains challenging with short reads. Rather, we have shown how the impact of SVs can be assayed without necessarily calling them, or mapping their breakpoints.

In this way, we can distinguish transpositions from local SVs, and determine the approximate locations of transpositions. The privileged role of the reference genome in the analysis means that some transpositions appear as deletions, so we probably have underestimated their true frequency. Nevertheless, a quarter of the SVs we detected are transpositions. Given the large numbers of transposable elements in *Arabidopsis* [$>11,000$ from >300 families are annotated in the reference (Quadrona *et al.* 2016)], this is unsurprising. However, many of the SVs we mapped are too large, covering tens of kilobases, to be single transposon-mediated events.

In the minority of cases where we could delineate breakpoints exactly, we often found SVs are complex combinations of different SV types. More often, breakpoints are not simple cut-and-paste transformations of the reference genome, as illustrated in Figure 6C. Indeed, it is frequently impossible to determine precisely the changes that led to many observed structural variants.

Because we used ultra-low-coverage $0.3\times$ sequence data, we divided the *Arabidopsis* genome into 10 kb bins when counting read-mapping anomalies. With higher coverage and a larger sample size, it would be possible to use a larger number of narrower bins, thereby improving resolution. The release of >3000 rice genomes sequenced at $\sim 14\times$ (Li *et al.* 2014), and >1000 *Arabidopsis* accessions sequenced at over

~20× (Alonso-Blanco *et al.* 2016) means that there are now large collections of inbred plant genomes available for analysis. Both of these sets are worldwide surveys of germplasm, in which we expect SVs to contribute significantly to, and be confounded with, their extensive population structure, in contrast to the MAGIC population used here. Disentangling these effects will be a challenging but important task.

Similarly, extending this methodology to outbred individuals, either descended from inbred strains [such as the mouse diversity outcross, DO (Svenson *et al.* 2012)], or natural populations, such as humans, requires modification. Heterozygous loci may carry different SVs with different SV-QTL. It is likely that a population with a limited haplotype space, like the DO, will be less challenging to map than will natural populations containing many low-frequency SVs associated with mobile elements. Large populations of sequenced humans are now available (Cai *et al.* 2015), making such investigations possible.

Mapping SVs as traits in a population brings new insights to the problem of QTL analysis. First, an SV trait inside a QTL may entirely explain the genetic effect at the QTL, and hence provide support for being the causal variant (*e.g.*, Figure 5). Second, SV traits are much more tightly localized than are QTL: there is little or no correlation between neighboring SV traits, so there are no effects of linkage disequilibrium. Our analysis also shows that expression of genes is often dysregulated or even silenced within large SVs, suggesting that an SV causes multiple regulatory and phenotypic effects.

Finally, even in a population like *Arabidopsis* MAGIC where the local haplotype space is known, structural variation has an impact on heritability that cannot be explained by standard genetic variation. This is unexpected given the breeding history and genetic architecture of the MAGIC lines, for, if an SV segregated among the founders of the MAGIC lines, then it should be tagged by the local haplotype context, and therefore contribute to both h_H^2 and h_{SV}^2 .

One possible explanation is that structural variation at loci rich in mobile elements accumulates independently within each lineage, leading to SVs that are private to each MAGIC line but tend to occur at the same loci, thereby creating similar phenotypic effects. Supporting this, in our analysis, the SV-relationship matrix is calculated empirically, without regard to the ancestry of the MAGIC lines, being solely a function of the correlations of read-mapping anomalies. Therefore, recalling that the history of each MAGIC line includes a private lineage of at least five generations of selfing, were SVs to accumulate recurrently, but independently, in different lineages, then these could generate phenotypic associations invisible to SNP or haplotype variation. In *Arabidopsis*, some mobile elements are methylated, often in response to environmental cues, and this methylation plays a role in the epigenetic control of certain phenotypes (Ito and Kakutani 2014). This effect might contribute to the heritability associated with structural variation observed here. Testing this hypothesis in *Arabidopsis* MAGIC lines would require complete and precise reassembly of each genome using long reads, annotation of mobile elements, and determination of their methylation status.

The role that recurrent, but independent, genomic rearrangements might play in *Arabidopsis*, and in other species remains to be seen, but there is no *a priori* reason why it should not drive phenotypic variation. The unstable inheritance of 45S rDNA genes in *Arabidopsis* lends support to this view (Rabanal *et al.* 2017). The approach used here may therefore have wider application to other populations to characterize the impact of cryptic structural variation on phenotypes.

Acknowledgments

We thank Fernando Rabanal for comments on the manuscript. M.I. and R.M. were supported by the Wellcome Trust Core Award grant 090532/Z/09/Z. M.I. was supported by a grant from the UK Engineering and Physical Sciences Research Council. R.M.C. was supported by National Science Foundation grant 0929262. E.J.O. and R.G. were supported by National Institutes of Health Genetics training grant T32 GM-007464.

Literature Cited

- Alonso-Blanco, C., J. Andrade, C. Becker, F. Bemm, J. Bergelson *et al.*, 2016 1,135 Genomes reveal the global pattern of polymorphism in *Arabidopsis thaliana*. *Cell* 166: 481–491.
- Berlin, K., S. Koren, C.-S. Chin, J. P. Drake, J. M. Landolin *et al.*, 2015 Assembling large genomes with single-molecule sequencing and locality-sensitive hashing. *Nat. Biotechnol.* 33: 623–630 (erratum: *Nat. Biotechnol.* 33: 1109).
- Cabrera, C. P., P. Navarro, J. E. Huffman, A. F. Wright, C. Hayward *et al.*, 2012 Uncovering networks from genome-wide association studies via circular genomic permutation. *G3* 2: 1067–1075.
- Cai, N., T. B. Bigdeli, W. Kretzschmar, Y. Li, J. Liang *et al.*, 2015 Sparse whole-genome sequencing identifies two loci for major depressive disorder. *Nature* 523: 588–591.
- Cao, J., K. Schneeberger, S. Ossowski, T. Gunther, S. Bender *et al.*, 2011 Whole-genome sequencing of multiple *Arabidopsis thaliana* populations. *Nat. Genet.* 43: 956–963.
- Chaisson, M. J., and G. Tesler, 2012 Mapping single molecule sequencing reads using basic local alignment with successive refinement (BLASR): application and theory. *BMC Bioinformatics* 13: 238.
- Chen, K., J. W. Wallis, M. D. McLellan, D. E. Larson, J. M. Kalicki *et al.*, 2009 BreakDancer: an algorithm for high-resolution mapping of genomic structural variation. *Nat. Methods* 6: 677–681.
- Davies, R. W., J. Flint, S. Myers, and R. Mott, 2016 Rapid genotype imputation from sequence without reference panels. *Nat. Genet.* 48: 965–969.
- Dudbridge, F., and B. P. C. Koeleman, 2004 Efficient computation of significance levels for multiple associations in large studies of correlated data, including genomewide association studies. *Am. J. Hum. Genet.* 75: 424–435.
- Durbin, R. M., G. R. Abecasis, D. L. Altshuler, A. Auton, L. D. Brooks *et al.*, 2010 A map of human genome variation from population-scale sequencing. *Nature* 467: 1061–1073.
- Durkin, K., W. Coppieters, C. Drögemüller, N. Ahariz, N. Cambisano *et al.*, 2012 Serial translocation by means of circular intermediates underlies colour sidedness in cattle. *Nature* 482: 81–84.
- Franz, P. F., S. Armstrong, J. H. de Jong, L. D. Parnell, C. van Drunen *et al.*, 2000 Integrated cytogenetic map of chromosome arm 4S of *A. thaliana*: structural organization of heterochromatic knob and centromere region. *Cell* 100: 367–376.

- Gan, X., O. Stegle, J. Behr, J. G. Steffen, P. Drewe *et al.*, 2011 Multiple reference genomes and transcriptomes for *Arabidopsis thaliana*. *Nature* 477: 419–423.
- Genovese G., R. E. Handsaker, H. Li, N. Altemose, A. M. Lindgren *et al.*, 2013 Using population admixture to help complete maps of the human genome. *Nat. Genet.* 45: 406–414, 414e1–414e2.
- Hu, T. T., P. Pattyn, E. G. Bakker, J. Cao, J.-F. Cheng *et al.*, 2011 The *Arabidopsis lyrata* genome sequence and the basis of rapid genome size change. *Nat. Genet.* 43: 476–481.
- Ito, H., and T. Kakutani, 2014 Control of transposable elements in *Arabidopsis thaliana*. *Chromosome Res.* 22: 217–223.
- Jain, M., I. T. Fiddes, K. H. Miga, H. E. Olsen, B. Paten *et al.*, 2015 Improved data analysis for the MinION nanopore sequencer. *Nat. Methods* 12: 351–356.
- Jean, G., A. Kähles, V. T. Sreedharan, F. De Bona, and G. Rätsch, 2010 RNA-Seq read alignments with PALMapper. *Curr. Protoc. Bioinformatics.* 11: Unit 11.6.
- Kang, H. M., N. A. Zaitlen, C. M. Wade, A. Kirby, D. Heckerman *et al.*, 2008a Efficient control of population structure in model organism association mapping. *Genetics* 178: 1709–1723.
- Kang, H. M., C. Ye, and E. Eskin, 2008b Accurate discovery of expression quantitative trait loci under confounding from spurious and genuine regulatory hotspots. *Genetics* 180: 1909–1925.
- Kemen, E., A. Gardiner, T. Schultz-Larsen, A. C. Kemen, A. L. Balmuth *et al.*, 2011 Gene gain and loss during evolution of obligate parasitism in the white rust pathogen of *Arabidopsis thaliana*. *PLoS Biol.* 9: e1001094.
- Kent, W. J., 2002 BLAT—the BLAST-like alignment tool. *Genome Res.* 12: 656–664.
- Kover, P. X., W. Valdar, J. Trakalo, N. Scarcelli, I. M. Ehrenreich *et al.*, 2009 A multiparent advanced generation inter-cross to fine-map quantitative traits in *Arabidopsis thaliana*. *PLoS Genet.* 5: e1000551.
- Kronenberg, Z. N., E. J. Osborne, K. R. Cone, B. J. Kennedy, E. T. Domyan *et al.*, 2015 Wham: identifying structural variants of biological consequence. *PLoS Comput. Biol.* 11: e1004572.
- Lai, A. G., M. Denton-Giles, B. Mueller-Roeber, J. H. Schippers, and P. P. Dijkwel, 2011 Positional information resolves structural variations and uncovers an evolutionarily divergent genetic locus in accessions of *Arabidopsis thaliana*. *Genome Biol. Evol.* 3: 627–640.
- Layer, R. M., C. Chiang, A. R. Quinlan, and I. M. Hall, 2014 LUMPY: a probabilistic framework for structural variant discovery. *Genome Biol.* 15: R84.
- Li, H., and R. Durbin, 2010 Fast and accurate long-read alignment with Burrows-Wheeler transform. *Bioinformatics* 26: 589–595.
- Li, J.-Y., J. Wang, and R. S. Zeigler, 2014 The 3,000 rice genomes project: new opportunities and challenges for future rice research. *Gigascience* 3: 8.
- Long, Q., F. A. Rabanal, D. Meng, C. D. Huber, A. Farlow *et al.*, 2013 Massive genomic variation and strong selection in *Arabidopsis thaliana* lines from Sweden. *Nat. Genet.* 45: 884–890.
- Lunter, G., and M. Goodson, 2011 Stampy: a statistical algorithm for sensitive and fast mapping of illumina sequence reads. *Genome Res.* 21: 936–939.
- Manske, H. M., and D. P. Kwiatkowski, 2009 LookSeq: a browser-based viewer for deep sequencing data. *Genome Res.* 19: 2125–2132.
- McKenna, A., M. Hanna, E. Banks, A. Sivachenko, K. Cibulskis *et al.*, 2010 The genome analysis toolkit: a MapReduce framework for analyzing next-generation DNA sequencing data. *Genome Res.* 20: 1297–1303.
- Mills, R. E., K. Walter, C. Stewart, R. E. Handsaker, K. Chen *et al.*, 2011 Mapping copy number variation by population-scale genome sequencing. *Nature* 470: 59–65.
- Nicod, J., R. W. Davies, N. Cai, C. Hassett, L. Goodstadt *et al.*, 2016 Genome-wide association of multiple complex traits in outbred mice by ultra-low-coverage sequencing. *Nat. Genet.* 48: 912–918.
- Nishimura, N., M. Okamoto, M. Narusaka, M. Yasuda, H. Nakashita *et al.*, 2009 ABA hypersensitive germination2–1 causes the activation of both abscisic acid and salicylic acid responses in *Arabidopsis*. *Plant Cell Physiol.* 50: 2112–2122.
- Quadrona, L., A. Bortolini Silveira, G. F. Mayhew, C. LeBlanc, R. A. Martienssen *et al.*, 2016 The *Arabidopsis thaliana* mobilome and its impact at the species level. *Elife* 5: e15716.
- Rabanal, F. A., N. Viktoria, M. Terezia, P. Y. Novikova, M. Lysak, R. Mott, and M. Nordborg, 2017 Unstable Inheritance of 45S rRNA genes in *Arabidopsis thaliana*. *G3: Genes, Genomes, Genetics* DOI: 10.1534/g3.117.040204.
- Rausch, T., T. Zichner, A. Schlattl, A. M. Stütz, V. Benes *et al.*, 2012 DELLY: structural variant discovery by integrated paired-end and split-read analysis. *Bioinformatics* 28: i333–i339.
- Rimmer, A., H. Phan, I. Mathieson, Z. Iqbal, S. R. F. Twigg *et al.*, 2014 Integrating mapping-, assembly- and haplotype-based approaches for calling variants in clinical sequencing applications. *Nat. Genet.* 46: 912–918.
- Rozen, S., and H. Skaletsky, 2000 Primer3 on the WWW for general users and for biologist programmers. *Methods Mol. Biol.* 132: 365–386.
- Simpson, J. T., and M. Pop, 2015 The theory and practice of genome sequence assembly. *Annu. Rev. Genomics Hum. Genet.* 16:153–172.
- Simpson, J. T., R. E. McIntyre, D. J. Adams, and R. Durbin, 2010 Copy number variant detection in inbred strains from short read sequence data. *Bioinformatics* 26: 565–567.
- Sindi, S. S., S. Onal, L. C. Peng, H.-T. Wu, and B. J. Raphael, 2012 An integrative probabilistic model for identification of structural variation in sequencing data. *Genome Biol.* 13: R22.
- Springate, D. A., and P. X. Kover, 2014 Plant responses to elevated temperatures: a field study on phenological sensitivity and fitness responses to simulated climate warming. *Glob. Chang. Biol.* 20: 456–465.
- Svenson, K. L., D. M. Gatti, W. Valdar, C. E. Welsh, R. Cheng *et al.*, 2012 High-resolution genetic mapping using the Mouse Diversity outbred population. *Genetics* 190: 437–447.
- Thines, M., Y. J. Choi, E. Kemen, S. Ploch, E. B. Holub *et al.*, 2009 A new species of Albugo parasitic to *Arabidopsis thaliana* reveals new evolutionary patterns in white blister rusts (Albuginaceae). *Persoonia* 22: 123–128.
- Van Der Biezen, E. A., C. T. Freddie, K. Kahn, J. E. Parker, and J. D. G. Jones, 2002 *Arabidopsis* RPP4 is a member of the RPP5 multigene family of TIR-NB-LRR genes and confers downy mildew resistance through multiple signalling components. *Plant J.* 29: 439–451.
- Wijnker, E., G. Velikkakam James, J. Ding, F. Becker, J. R. Klasek *et al.*, 2013 The genomic landscape of meiotic crossovers and gene conversions in *Arabidopsis thaliana*. *Elife* 2: e01426.
- Yalcin, B., K. Wong, A. Agam, M. Goodson, T. M. Keane *et al.*, 2011 Sequence-based characterization of structural variation in the mouse genome. *Nature* 477: 326–329.
- Ye, K., M. H. Schulz, Q. Long, R. Apweiler, and Z. Ning, 2009 Pindel: a pattern growth approach to detect break points of large deletions and medium sized insertions from paired-end short reads. *Bioinformatics* 25: 2865–2871.
- Yi, H., and E. J. Richards, 2009 Gene duplication and hypermutation of the pathogen Resistance gene SNC1 in the *Arabidopsis* bal variant. *Genetics* 183: 1227–1234.

Communicating editor: T. F. C. Mackay

GENETICS

Supporting Information

www.genetics.org/lookup/suppl/doi:10.1534/genetics.116.192823/-/DC1

Genomic Rearrangements in *Arabidopsis* Considered as Quantitative Traits

Martha Imprialou, André Kahles, Joshua G. Steffen, Edward J. Osborne, Xiangchao Gan, Janne Lempe, Amarjit Bhomra,
Eric Belfield, Anne Visscher, Robert Greenhalgh, Nicholas P Harberd, Richard Goram, Jotun Hein, Alexandre Robert-
Seilaniantz, Jonathan Jones, Oliver Stegle, Paula Kover, Miltos Tsiantis, Magnus Nordborg, Gunnar Rättsch, Richard M. Clark
and Richard Mott